Growth and characterization of large (Y,La)TiO_3 and (Y,Ca)TiO_3 single crystals

S. Hameed,[1,*] J. Joe,[1] L. R. Thoutam,[2,3] J. Garcia-Barriocanal,[4] B. Yu,[1] G. Yu,[4,5] S. Chi,[6] T. Hong,[6] T. J. Williams,[6] J. W. Freeland,[7] P. M. Gehring,[8] Z. Xu,[8,9] M. Matsuda,[6] B. Jalan,[2] and M. Greven[1,*]

[1]*School of Physics and Astronomy, University of Minnesota, Minneapolis, Minnesota 55455, USA*
[2]*Department of Chemical Engineering and Materials Science, University of Minnesota, Minneapolis, Minnesota 55455, USA*
[3]*Department of Electronics and Communications Engineering, SR University, Warangal Urban, Telangana 506371, India*
[4]*Characterization Facility, University of Minnesota, Minneapolis, Minnesota 55455, USA*
[5]*Informatics Institute, University of Minnesota, Minneapolis, Minnesota 55455, USA*
[6]*Neutron Scattering Division, Oak Ridge National Laboratory, Oak Ridge, Tennessee 37831, USA*
[7]*X-ray Science Division, Argonne National Laboratory, Argonne, Illinois 60439, USA*
[8]*NIST Center for Neutron Research, National Institute of Standards and Technology, Gaithersburg, Maryland 20899, USA*
[9]*Department of Materials Science and Engineering, University of Maryland, College Park, Maryland 20742, USA*

(Received 1 July 2021; accepted 2 December 2021; published 29 December 2021)

The Mott-insulating rare-earth titanates ($RTiO_3$, with R being a rare-earth ion) are an important class of materials that encompasses interesting spin-orbital phases as well as ferromagnet-antiferromagnet and insulator-metal transitions. The growth of these materials has been plagued by difficulties related to overoxidation, which arises from a strong tendency of Ti^{3+} to oxidize to Ti^{4+}. We describe our efforts to grow sizable single crystals of $YTiO_3$, $Y_{1-x}La_xTiO_3$ ($x \leqslant 0.25$), and $Y_{1-y}Ca_yTiO_3$ ($y \leqslant 0.35$) with the optical traveling-solvent floating-zone technique. We present sample characterization via chemical composition analysis, magnetometry, charge transport, neutron scattering, x-ray absorption spectroscopy, and x-ray magnetic circular dichroism to understand macroscopic physical property variations associated with overoxidation. Furthermore, we demonstrate a good signal-to-noise ratio in inelastic magnetic neutron scattering measurements of spin-wave excitations. A superconducting impurity phase, found to appear in Ca-doped samples at high doping levels, is identified as TiO.

DOI: 10.1103/PhysRevMaterials.5.125003

I. INTRODUCTION

The Mott-insulating rare-earth titanates $RTiO_3$ exhibit myriad magnetic and electronic phases as a result of strong coupling among spin, orbital, charge, and lattice degrees of freedom [1]. These oxides have a $GdFeO_3$-type distorted perovskite structure, with tilts and rotations of the oxygen octahedra that arise from the size mismatch between the R and Ti ions. The distortion, and the associated deviation of the Ti-O-Ti bond angle from 180°, increases with decreasing R-ion radius [2] and has a strong influence on the superexchange involving the Ti $3d$ t_{2g}^1 spin-1/2 moments. This leads to a rare antiferromagnetic-ferromagnetic phase transition/crossover; materials with a large R-ion radius (La, Sm, Nd, etc.) display an antiferromagnetic ground state, whereas those with a small R-ion radius (Y, Gd, Dy, etc.) display a ferromagnetic ground state [1,3,4]. The phase-transition/crossover can also be induced in solid-solution systems formed by isovalent substitution, e.g., $Y_{1-x}La_xTiO_3$ [5–8] and $Sm_{1-x}Gd_xTiO_3$ [9].

It is also possible to tune $RTiO_3$ from a Mott insulator to a metallic state via hole doping, which can be achieved by substituting the trivalent R^{3+} ion with a divalent A^{2+} ion such as Ca^{2+} or Sr^{2+} to form $R_{1-y}A_yTiO_3$. Intriguingly, the critical doping $y = y_c$ up to which the Mott-insulating state survives can be located significantly away from half filling ($y = 0$), with y_c ranging from 0.05 in $La_{1-y}Sr_yTiO_3$ [10] to 0.35 in $Y_{1-y}Ca_yTiO_3$ [11,12]. Recent work on $Y_{1-y}Ca_yTiO_3$ showed that this insulator-metal transition involves electronic phase separation [12].

Recent years have also witnessed a surge of interest in $RTiO_3$-based heterostructures in a search for novel electronic properties and correlated electronic states at interfaces [13–18]. For instance, a ferromagneticlike state was induced in a rare-earth nickelate ($RNiO_3$) by forming an interface with $GdTiO_3$ [18]. Another example is the control of charge carrier densities in $NdTiO_3/SrTiO_3$ heterostructures [13,14]. It has thus become increasingly important to fully characterize and understand the properties of the bulk compounds. One of the primary issues that has plagued the study of the electronic and magnetic properties of $RTiO_3$ is a strong tendency of Ti^{3+} to oxidize to Ti^{4+}, which makes it extremely difficult to obtain stoichiometric samples. Whereas this overoxidation effect can result from both cation vacancies and oxygen interstitials, the latter has been shown to be energetically favored [14]. The overoxidation effect has been the subject of recent studies, particularly of films, and it has been shown to significantly affect magnetic and electronic properties [19,20].

Here we describe our efforts to grow and thoroughly characterize large single crystals of La-substituted and Ca-doped $YTiO_3$ with the traveling-solvent floating-zone (TSFZ) technique. Our goal is to provide a comprehensive report

*Corresponding authors: hamee007@umn.edu, greven@umn.edu

on the growth of large single crystals of $Y_{1-x}La_xTiO_3$ and $Y_{1-y}Ca_yTiO_3$ to aid future studies of this important class of quantum materials, such as magnetic neutron scattering and muon spin rotation [8]. We refer to "substitution" in the case of isovalent La substitution to emphasize that this does not lead to charge-carrier doping, unlike the case of divalent Ca doping. We carefully characterize the changes in properties along large single crystals via chemical composition analysis, magnetometry, charge transport, elastic and inelastic neutron scattering, x-ray diffraction, x-ray absorption spectroscopy, and x-ray magnetic circular dichroism. We discuss the difficulties associated with obtaining homogeneous large single crystals and the procedure that we adopted to prepare sizable samples. We also identify and characterize a superconducting impurity phase of TiO that appears at large Ca-doping levels in $Y_{1-y}Ca_yTiO_3$. Some of the crystals investigated here were used in recent studies of the ferromagnet-antiferromagnet transition in $Y_{1-x}La_xTiO_3$ [8], the Mott insulator-metal transition in $Y_{1-y}Ca_yTiO_3$ [12], the effect of uniaxial strain on the magnetic ground state in these systems [21], and measurements of the spin waves in both systems [22].

This paper is organized as follows: Sec. II describes the single-crystal growth and experimental details. Sections III A, III B, and III C describe the characterization of single crystals of $YTiO_3$, $Y_{1-x}La_xTiO_3$, and $Y_{1-y}Ca_yTiO_3$, respectively. Section III D discusses sample characterization via elastic and inelastic neutron scattering. Finally, we summarize our main conclusions in Sec. IV.

II. EXPERIMENTAL METHODS

Single crystals of $Y_{1-x}La_xTiO_3$ ($x \leqslant 0.25$) and $Y_{1-y}Ca_yTiO_3$ ($y \leqslant 0.35$) were melt-grown with the TSFZ technique. The starting materials were La_2O_3, Y_2O_3, and Ti_2O_3 for $Y_{1-x}La_xTiO_3$ and Y_2O_3, $CaTiO_3$, and Ti_2O_3 for $Y_{1-y}Ca_yTiO_3$. In order to prevent the oxidation of Ti^{3+} to Ti^{4+}, we *started* with an oxygen-deficient composition, $Y_{1-x}La(Ca)_xTiO_{3-\delta}$, similar to that used in prior work [5,6]. This was achieved by adding Ti powder to the starting materials. The idea here is to compensate for residual oxygen in the furnace that could create oxygen interstitials in the grown crystal [14]. We emphasize that δ simply refers to the composition of the *starting* materials in the synthesis; this does not imply that the grown crystals have the same value of δ. The La_2O_3, $CaTiO_3$, and Y_2O_3 powders were predried in air at 1000 °C for 12 h. The starting materials were then mixed in the stoichiometric ratio $Y_{1-x}La(Ca)_xTiO_{3-\delta}$ and subsequently pressed at 70 MPa into two rods with a diameter of 6 mm and lengths of 20 and 100 mm for use as seed and feed rods, respectively. The feed and seed rods were then loaded into a Crystal Systems four-mirror optical TSFZ furnace [23]. The growths were performed at rates of 2 to 5 mm/h in a reducing atmosphere with a mixed gas of 5% H_2/95% Ar at a pressure of 5 bars in the case of the La-substituted system and pure Ar gas at a pressure of 5 bars in the case of the Ca-doped system. The growth chamber was flushed with the gas before the start of each growth. In the case of $YTiO_3$, a pyrochlore $Y_2Ti_2O_7$ impurity phase was observed to form in the absence of this flushing step due to the large amount of residual oxygen in the chamber. The choice of δ for different compositions is detailed below, in the respective sections.

Laue diffraction measurements confirmed the single-crystal nature of the samples and enabled the determination of the crystallographic axes. $YTiO_3$ and its La-substituted and Ca-doped variants have a *Pbnm* orthorhombic structure at room temperature. We use the orthorhombic notation throughout, indicated by the subscript "o." Chemical composition analysis was performed via wavelength-dispersive spectroscopy (WDS). Note that the oxygen off-stoichiometry cannot be obtained from WDS and therefore was not determined. Magnetic-susceptibility measurements were performed with a Quantum Design magnetic property measurement system (MPMS). For DC susceptibility measurements, we used the dc superconducting quantum interference device magnetometer, whereas AC susceptibility measurements were performed with a home-built probe that consists of two matched detection coils, with the excitation field provided by the built-in MPMS coil. The magnetic field was applied along the sample's c axis. Resistivity measurements for $YTiO_3$ were carried out with a Quantum Design PPMS Dynacool system. A Keithley 2612B sourcemeter was used in the four-wire configuration to source the current and measure the voltage. The samples were cut into a square shape with an ab plane surface, with the a and b axes being the sides of the square. The sample surfaces were polished with lapping films to 1 μm grade, and electrical contacts were made with gold wires and silver paint. All samples were measured in a van der Pauw geometry. X-ray absorption spectroscopy/x-ray magnetic circular dichroism (XAS/XMCD) measurements were carried out at beamline 4-ID-C of the Advanced Photon Source at Argonne National Laboratory. The measurements reported here were obtained in the bulk-sensitive total fluorescence yield (TFY) detection mode. Although measurements were performed in the surface-sensitive total electron yield (TEY) detection mode as well, the surfaces were found to be oxidized (see the Supplemental Material [24]). A reference $SrTiO_3$ sample was used to align the spectra energy scales to within 0.1 eV. The surfaces of the samples used for XAS/XMCD measurements were cut parallel to the (001) plane and polished to a roughness of $\sim$0.3 μm using polycrystalline diamond suspension. The x rays were incident at an angle of 30° with respect to the c axis. A 5-T magnetic field was applied along the x-ray beam for the XMCD measurements. X-ray diffraction (XRD) measurements were performed on a Bruker D8 Discover x-ray diffractometer, equipped with a Co $K\alpha$ x-ray source and a VANTE-500 area detector.

Neutron scattering experiments were performed with the HB-1 and HB-3 thermal triple-axis spectrometers and the CG-4C cold-triple axis spectrometer at the High Flux Isotope Reactor, Oak Ridge National Laboratory, and with the BT-7 thermal triple-axis spectrometer at the NIST Center for Neutron research. The final energies of the scattered neutrons were fixed at 14.7 meV for the thermal triple-axis measurements and at 4.5 meV for the cold triple-axis measurements. We used horizontal beam collimations of 48′-80′-sample-80′-120′ at HB-1 and HB-3, open-80′-sample-80′-120′ at BT-7, and open-open-sample-80′-open at CG-4C. In order to eliminate higher-order neutrons, PG filters were used at HB-1, HB-3, and BT-7, and a cooled Be filter was used at CG-4C. A ^{4}He

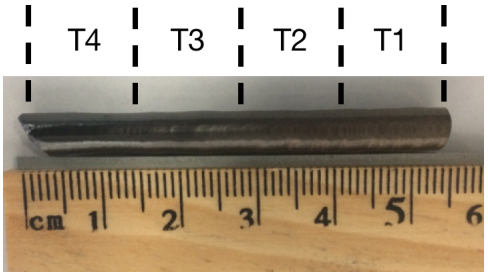

FIG. 1. Picture of a large $YTiO_3$ single crystal grown with the TSFZ method. The sectioning used for characterization is indicated.

cryostat was used to reach temperatures down to 1.5 K. The samples were mounted in the $(0KL)$ scattering plane.

III. RESULTS

A. Characterization of $YTiO_3$ single crystals

As detailed in Sec. II, we used an oxygen-deficient starting composition to grow the single crystals. In the case of $YTiO_3$, several different values of δ in the range 0–0.08 were attempted. We found that $\delta = 0.04$ yielded the highest Curie temperature of $T_C \sim 30$ K, as determined by magnetometry. For this step of optimizing δ in the growth process, we characterized a single-crystal piece picked from the end of the growth. However, as detailed below, we found that significant inhomogeneity exists in the magnetic and transport properties across the length of the growth.

Figure 1 shows an example of a large $YTiO_3$ single crystal. The characterization was performed by cutting the crystal into four approximately equal-length parts, as indicated in the figure. The naming convention here is such that the numbered suffix represents the position of the sample from the end of the growth. We characterized the samples using magnetometry, charge transport, chemical composition analysis, and XAS/XMCD.

Figure 2 shows the magnetic-field dependence of the magnetization M obtained at 5 K for the four $YTiO_3$ samples. The values of M obtained at 6.5 T are summarized in Table I. Whereas samples T1 and T2 are seen to exhibit closely similar $M(H)$ behaviors, a clear decrease in M is observed for sample T3, and an even further decrease is observed for T4. The inset in Fig. 2 displays the temperature dependence of the field-cooled magnetization obtained in an applied magnetic field of 50 G. The Curie temperature is defined as the midpoint of the transition observed in the M vs T curves and summarized in Table I. Samples T1 and T2 exhibit closely similar Curie temperatures, whereas a decrease in T_C is observed for sample T3, and a further decrease is observed for sample T4.

As a next characterization step, we measured the temperature dependence of the resistivity, as shown in Fig. 3. All samples display insulating behavior. Further, the temperature dependence of the resistivity is well fit to thermally activated behavior, $\rho \propto e^{-E_a/k_BT}$, in agreement with prior reports [4,7,25,26]. The underlying mechanism of the activated transport was recently shown to be small-hole-polaron hopping [26]. The room-temperature resistivity and the fit results for the activation energy E_a are displayed in Table I. The room-

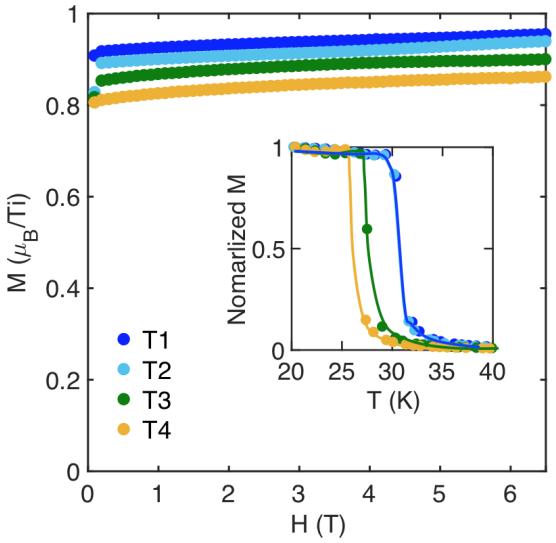

FIG. 2. Magnetic-field dependence of the magnetic moment per Ti ion for the $YTiO_3$ samples, obtained along the c axis at $T = 5$ K. The samples were zero-field cooled and measured in an increasing field. Inset: Temperature dependence of the field-cooled c-axis magnetization, obtained in an applied magnetic field of 50 G. The magnetization values are normalized to those at 20 K.

temperature resistivities of samples T3 and T4 are observed to be an order of magnitude lower than those of samples T1 and T2. Furthermore, samples T3 and T4 exhibit lower activation energies.

In order to understand the origin of the different magnetic and transport properties obtained for the $YTiO_3$ samples, we carried out a detailed chemical composition analysis using WDS. The results are summarized in Table I. Note that the uncertainties indicated for the Y:Ti ratio are standard uncertainties determined by measuring the composition at five different spots on the sample. The Y:Ti ratio for samples T1, T2, and T3 are observed to be similar, within error, whereas sample T4 has a slightly lower Y:Ti ratio. However, as seen from transport and magnetometry measurements, a clear difference exists between the properties of sample T3 and samples T1 and T2. Therefore, the observed differences cannot be entirely due to a slightly different Y:Ti ratio, which points to the possibility of oxygen interstitials, the formation of which was previously shown to be energetically favorable in the $RTiO_3$ class of materials [13]. Unfortunately, this

TABLE I. Measured chemical composition, Curie temperature, magnetic moment at 5 K and 6.5 T, transport activation energy, and room-temperature resistivity for the four segments of the $YTiO_3$ crystal.

Sample	Y:Ti	T_C (K)	FM moment (μ_B/Ti)	E_a (meV)	ρ (300 K) (Ω cm)
T1	0.964(7)	30.8(4)	0.96(2)	316.8(8)	260(5)
T2	0.978(8)	30.8(4)	0.94(1)	295.4(8)	112(3)
T3	0.965(9)	27.5(5)	0.90(1)	219.9(4)	11.2(2)
T4	0.944(4)	26.5(5)	0.86(1)	221.3(9)	15.5(5)

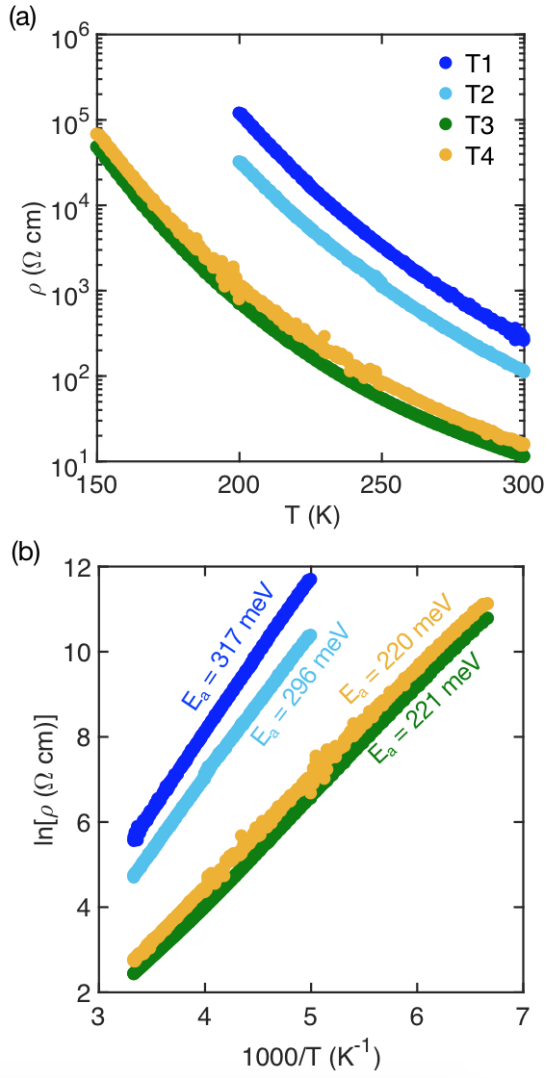

FIG. 3. (a) Temperature dependence of the resistivity for the $YTiO_3$ samples. (b) Arrhenius plot for the resistivities in (a), along with the corresponding activation energies.

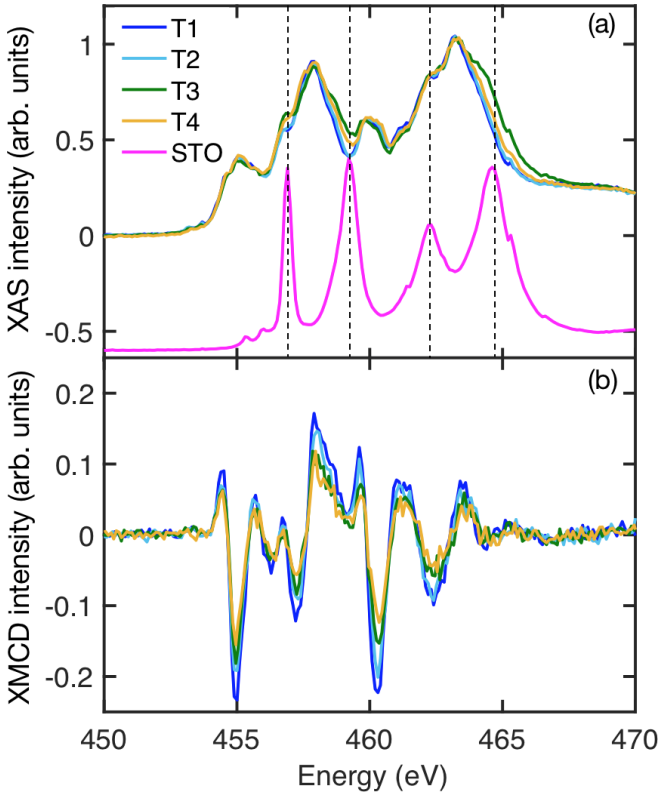

FIG. 4. (a) Ti $L_{2,3}$-edge XAS results for four $YTiO_3$ samples. The data measured at the lowest energy were subtracted, and the net intensity was subsequently normalized at the highest peak. A Ti^{4+} reference spectrum obtained from a $SrTiO_3$ (STO) sample is displayed as well; it has been shifted vertically for clarity, and the dashed black lines correspond to its peak positions. (b) XMCD intensities at the Ti $L_{2,3}$ edge at 6 K, in the ferromagnetic phase. The data were normalized by the intensity of the largest Ti $L_{2,3}$-edge XAS peak.

information is not accessible via WDS. Since both cation vacancies and oxygen interstitials would lead to a conversion from Ti^{3+} to Ti^{4+}, we attempted to characterize the extent of such overoxidation using XAS, as described below.

XAS is a powerful technique capable of distinguishing different valence states of elements. Figure 4(a) shows the XAS spectra obtained at the Ti $L_{2,3}$ edge. Clearly, the XAS spectra for samples T1 and T2 approximately coincide, whereas samples T3 and T4 display comparatively broadened peaks. A comparison with reference Ti^{4+} spectra obtained for a $SrTiO_3$ single crystal clearly indicates that the additional XAS intensity in samples T3 and T4 appears in the energy range associated with the Ti^{4+} spectral peaks, indicative of an overoxidation in samples T3 and T4. Such a partial conversion of Ti^{3+} to Ti^{4+} was reported in several other XAS works on the $RTiO_3$ class of materials [19,20,27]. In order to confirm the effect of such oxidation on the magnetic properties, we performed XMCD measurements at 6 K, deep in the ferromagnetic phase. As seen in Fig. 4(b), a gradual reduction in the XMCD signal is observed from sample T1 to sample T4, indicative of a weakening of the magnetic order, in agreement with the magnetometry data (Fig. 2).

Our results clearly illustrate that overoxidation via formation of cation vacancies or oxygen interstitials can strongly affect the magnetic and transport properties of $YTiO_3$. It must be noted, however, that there could be additional causes of these differences, such as extrinsic inhomogeneous strains that may nucleate across a large single crystal during growth. Ideally, such strain would be removed by annealing. However, the extreme tendency of Ti^{3+} to convert to Ti^{4+} in the presence of traces of oxygen renders such annealing processes extremely difficult for these materials.

B. Characterization of $Y_{1-x}La_xTiO_3$ single crystals

For the growth of $Y_{1-x}La_xTiO_3$ single crystals, we fixed δ at 0.04, i.e., the same value as for $YTiO_3$ in order to avoid property changes due to differences in oxygen off-stoichiometry in the starting material composition [8]. Intriguingly, however, we found that, at large x, the changes in T_C along the growth axis can be particularly severe. We present here the characterization of a crystal with $x = 0.22$.

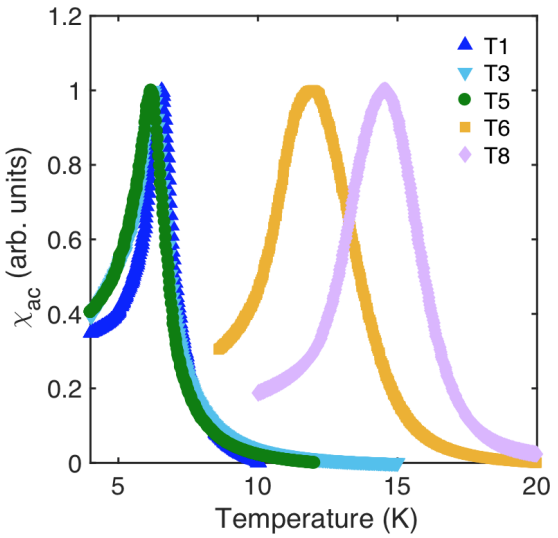

FIG. 5. Temperature dependence of the AC susceptibility obtained with an excitation frequency of 3.63 kHz for samples cut from a large $Y_{1-x}La_xTiO_3$ ($x = 0.22$) single crystal.

Similar to the case of $YTiO_3$ (Fig. 1), a 4-cm-long crystal was sectioned into approximately equal parts (eight instead of four, in this case). As before, T1 refers to the sample at the end of the growth; T8 refers to the sample near the beginning of the growth.

Figure 5 shows the temperature dependence of the AC magnetic susceptibility for five such samples. T_C, defined here as the temperature of the susceptibility peak, is summarized in Table II. Samples T1, T3, and T5 show similar T_C values, whereas samples T6 and T8 exhibit Curie temperatures that are more than a factor of 2 higher. Such a large change in T_C across the growth length was observed for La substitution levels in the range $x = 0.15$–0.25 (see the Supplemental Material [24]). Similar to the $YTiO_3$ characterization, we also measured the chemical composition of the samples across the length of the growth. This is summarized in Table II. Clearly, no significant differences are observed in the cation ratios, which brings us to the conclusion that the significant differences in magnetic properties are likely associated with oxygen interstitials. This is, perhaps, not surprising, given the extreme sensitivity of the magnetic and transport properties of $LaTiO_3$ to oxygen interstitials [28]. Yet, similar to $YTiO_3$, for sufficiently long growths, we found that an extended region of nearly constant T_C exists toward the latter part of the growth. However, as demonstrated in the present work, careful characterization needs to be performed to minimize the effects of overoxidation-related inhomogeneity, particularly when selecting large samples for neutron measurements. Note that, unlike the case of $YTiO_3$, the "stable" latter part of the growth has a lower T_C compared with the rest. For the preliminary inelastic neutron measurements of the spin-wave spectra at large La-substitution levels discussed below, we used samples from the latter parts of the growths that exhibit a nearly constant T_C. Given the strong suppression of the ordered moments with increasing La substitution [8], it was necessary to comount samples from many different growths in order to obtain a sufficiently large signal-to-noise ratio (see Fig. 6).

TABLE II. Chemical composition and Curie temperatures of $Y_{1-x}La_xTiO_3$ single-crystal samples with nominal composition $x = 0.22$. The chemical composition of sample T5 was not determined.

Sample	x	(Y+La):Ti	T_C (K)
T1	0.236(2)	0.978(18)	6.5(1)
T3	0.232(2)	0.983(12)	6.2(1)
T5			6.2(1)
T6	0.232(1)	0.984(4)	12.0(5)
T8	0.236(4)	0.976(9)	14.5(3)

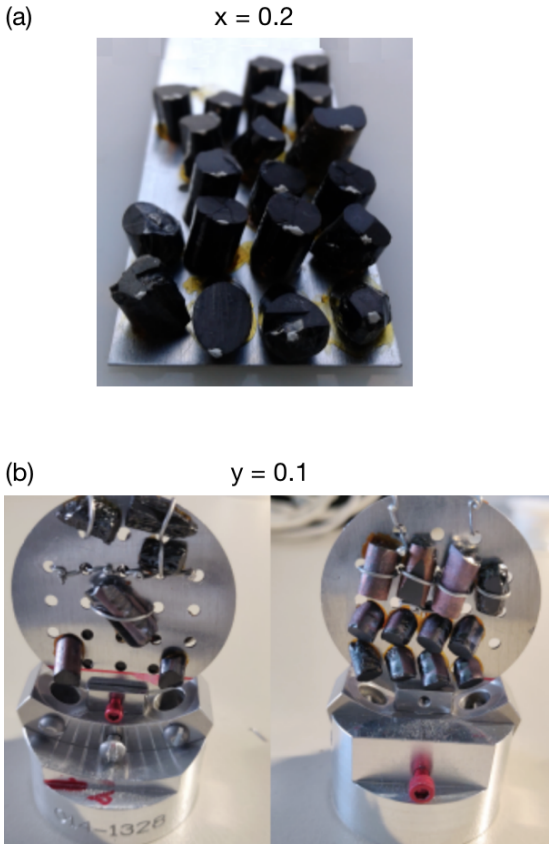

FIG. 6. Pictures of comounted single crystals of (a) $Y_{1-x}La_xTiO_3$ ($x = 0.2$) and (b) $Y_{1-y}Ca_yTiO_3$ ($y = 0.1$) for inelastic magnetic neutron scattering measurements.

C. Characterization of $Y_{1-y}Ca_yTiO_3$ single crystals

The $Y_{1-y}Ca_yTiO_3$ growth and characterization results differed from those for $Y_{1-x}La_xTiO_3$ in a number of ways. First, several attempts to grow single crystals with $y = 0.05$ and $\delta = 0.04$ failed and yielded only polycrystalline material. In order to obtain single crystals, it was found to be necessary to increase δ with increasing y. Part of the reason for this is most likely the higher melt temperature of the Ca-doped variant, which apparently leads to a stronger oxidizing effect [29]. The values of δ used ranged from 0.04 for $y = 0$ to 0.12 for $y = 0.5$. Unlike for the La-substituted system, however, Curie-temperature measurements revealed no significant

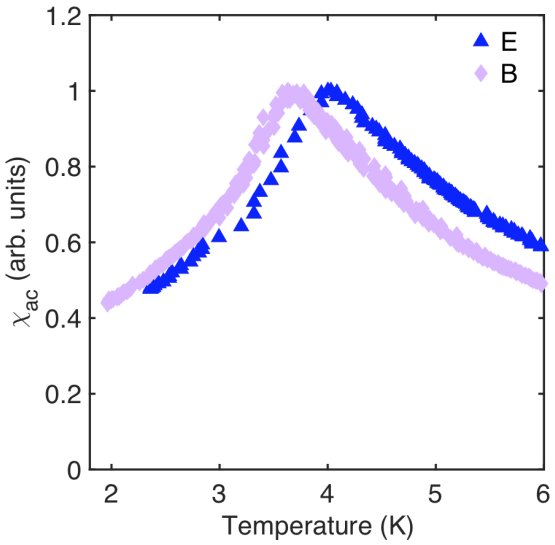

FIG. 7. Temperature dependence of the AC susceptibility obtained with an excitation frequency of 3.63 kHz for samples from near the beginning (B) and end (E) of the growth of a large $Y_{1-y}Ca_yTiO_3$ ($y = 0.15$) single crystal.

inhomogeneity along large single crystals of $Y_{1-y}Ca_yTiO_3$, even at relatively high doping levels. As an example, Fig. 7 shows the temperature dependence of the AC susceptibility for two samples from a large (about 4 cm long) $y = 0.15$ single crystal. Here, sample B is from a region near the beginning of the growth, whereas sample E is from a region near the end of the growth. Only a small difference in T_C ($\sim$0.3 K, i.e., less than 10%), identified from the position of the susceptibility peak, is observed. Data for additional doping levels up to $y = 0.2$ can be found in the Supplemental Material [24].

At high Ca-doping levels ($y \gtrsim 0.35$), a polycrystalline impurity phase was revealed by powder rings in XRD data [Fig. 8(a)]. The impurity peaks match those of cubic TiO with a lattice parameter of 4.260(3) Å [Fig. 8(b)]. This impurity phase exhibits a superconducting (SC) transition, as discerned from the diamagnetic signal in magnetometry measurements [Fig. 8(c)]. Interestingly, although we estimate the low-temperature volume fraction $4\pi\chi$ of the SC phase to be less than 2%, transport measurements using a van der Pauw geometry on some samples show a complete transition (in one of the directions) into a zero-resistance state [Fig. 8(c)]. This is likely due to the fact that the equipotential lines originating

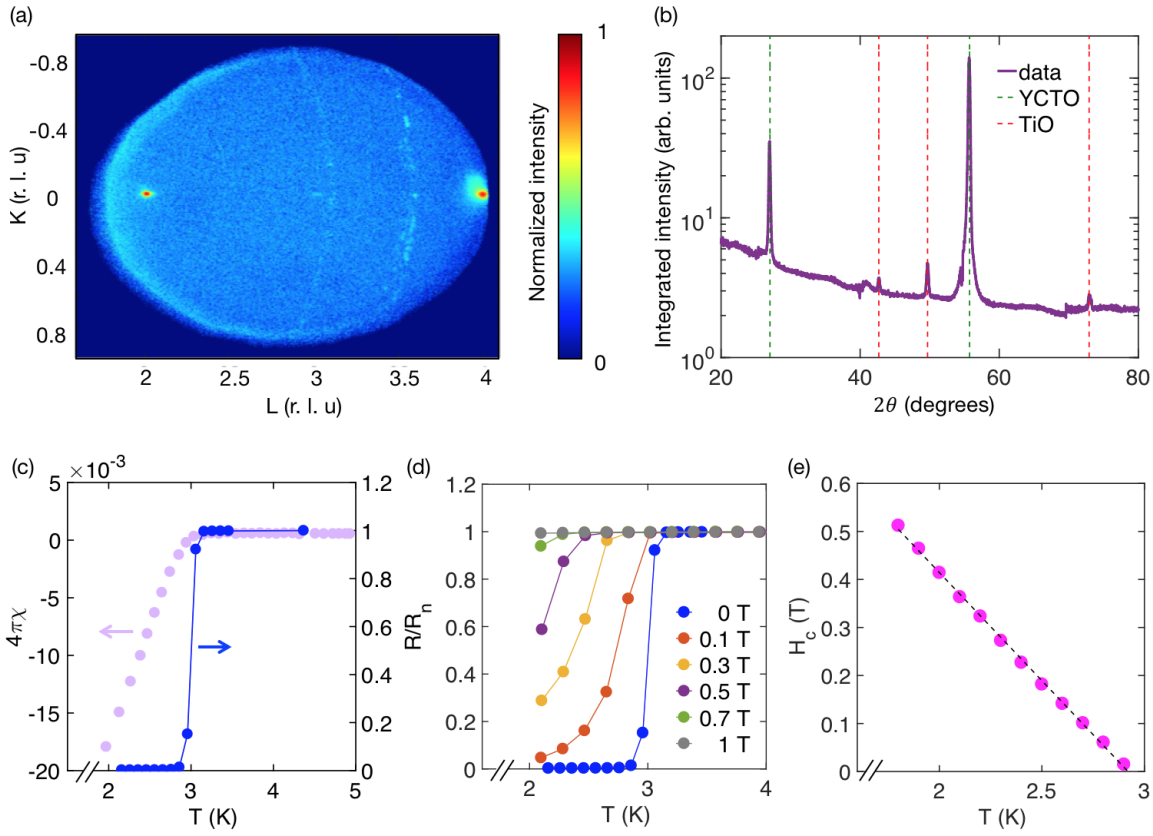

FIG. 8. (a) Reciprocal space map of the XRD intensity in the $(0KL)$ plane for a $Y_{1-y}Ca_yTiO_3$ (YCTO) single crystal with $y = 0.35$. Apart from the strong Bragg peaks at even integer valued K and L, powder rings due to a polycrystalline impurity phase are visible. The intensity has been normalized to the peak value at $(002)_o$. (b) Integrated XRD intensity as a function of the scattering angle 2θ for the same $y = 0.35$ crystal as in (a). The calculated 2θ values along with those for the TiO impurity phase are indicated as dashed lines. (c) Temperature dependence of the superconducting volume fraction $4\pi\chi$ obtained from zero-field-cooled magnetization in an applied c-axis magnetic field of 50 G (left axis) and of the sample resistance R, normalized to the normal-state value R_n (right axis). The onset temperatures are nearly indistinguishable. The data are for a $y = 0.4$ sample. Temperature dependence (d) of the normalized resistance in different applied magnetic fields and (e) of the critical magnetic field for the same sample as in (c).

from the voltage measurement contacts can be very close far away from the contacts in a van der Pauw geometry. This increases the chances that small SC regions will be captured by the measurement, as they short the equipotential lines [30,31]. This allowed us to characterize the SC properties of the TiO phase [Figs. 8(c)–8(e)]. We find a SC transition temperature of about 3 K, as defined by the midpoint of the transition [Fig. 8(c)]. This is consistent with literature values, which range from 0.5 to 7.4 K depending on growth conditions [32,33]. Interestingly, the resistive transition in Fig. 8(c) is sharper than in recent reports for nominally pure TiO in crystalline and film forms [32,33]. This is likely due to the difference in contact geometry since the prior work used the standard four-probe technique, which averages over the sample volume [32,33]. We also determined the temperature dependence of the critical magnetic field [Figs. 8(d) and 8(e)], defined here as the field at which the resistance recovers to 50% of the normal-state value. We observe a linear temperature dependence down to the lowest measured temperature (1.8 K), in agreement with recent work [32].

D. Neutron scattering measurements

As noted, one goal of the present work was to grow sizable single crystals of $Y_{1-x}La_xTiO_3$ and $Y_{1-y}Ca_yTiO_3$ for magnetic neutron scattering studies. Prior neutron scattering studies were restricted to the parent compounds $YTiO_3$ and $LaTiO_3$ [34,35]. Here we present neutron scattering data that demonstrate the good quality of our La-substituted and Ca-doped $YTiO_3$ crystals. Figure 9(a) displays rocking scans across the $(020)_o$ nuclear Bragg peak for single crystals with different chemical compositions. The crystal volumes were in the 0.7–0.8 cm^3 range, corresponding to a mass of about 4 g. Clearly, the crystal mosaic, defined here as the full width at half maximum (FWHM) of Gaussian fits, is less than 0.5°, indicative of high crystalline quality. Note that part of the broadening is associated with the instrumental resolution. Therefore, the FWHM represents an upper bound on the crystal mosaic. Figure 9(b) displays spin-wave data at $(001)_o$ for several single crystals. We observe a strong suppression of the spin-wave intensity, both with increasing La substitution and increasing Ca doping. In order to obtain a good signal-noise ratio for $x \geqslant 0.2$ and $y \geqslant 0.1$, we co-mounted ∼20 crystals with total masses in the 12–15 g range (Fig. 6). Detailed spin-wave measurements will be reported elsewhere [22].

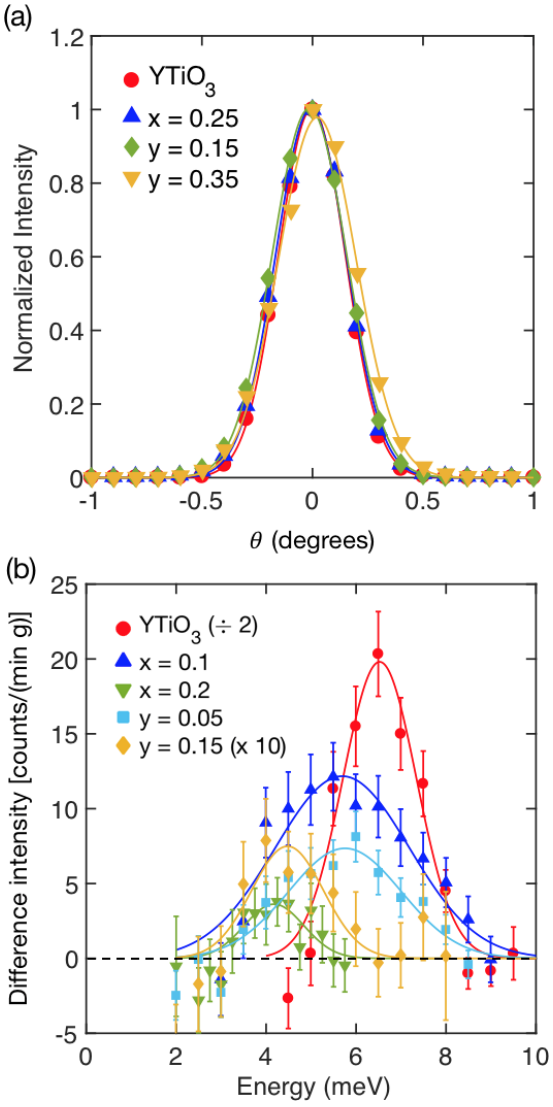

FIG. 9. (a) Neutron diffraction rocking scans across the $(020)_o$ Bragg peak for large single crystals of $Y_{1-x}La_xTiO_3$ and $Y_{1-y}Ca_yTiO_3$. The intensities are normalized to the peak values. The solid lines are Gaussian fits to the data. (b) Inelastic neutron scattering measurement of spin waves at $(001)_o$. The high-temperature ($T > T_C$) paramagnetic scattering was subtracted from data taken in the ferromagnetically ordered state at 1.5 K. Note that some of the data are scaled, as indicated. The error bars correspond to one standard deviation. The solid lines are guides to the eye.

IV. CONCLUSIONS

To summarize, we have successfully grown large single crystals of $YTiO_3$ and its La-substituted and Ca-doped variants with the TSFZ technique. From detailed characterization measurements, we found that inhomogeneous overoxidation can appear along large single crystals and strongly affects the magnetic and transport properties. This indicates that great care must be taken in preparing samples for experimental studies aimed to understand the phase diagram. We have demonstrated that it is possible to obtain elastic and inelastic magnetic neutron scattering data with good signal-to-noise ratios. We have also found a superconducting TiO polycrystalline impurity phase at large Ca-substitution levels. The superconducting transition temperature of this phase is about 3 K, and the critical magnetic field exhibits a linear temperature dependence, consistent with prior results for bulk and film samples.

ACKNOWLEDGMENTS

We thank K. Olson for help with the growth of the $Y_{1-x}La_xTiO_3$ ($x = 0.22$) crystal and A. Najev for helpful comments on the manuscript. The work at the University of Minnesota was funded by the Department of Energy through the University of Minnesota Center for Quantum Materials,

under Grant No. DE-SC0016371. Parts of this work were carried out in the University of Minnesota Characterization Facility, which receives partial support from NSF through the MRSEC program. Electron microprobe analysis of the crystal chemical composition was carried out at the Electron Microprobe Laboratory, Department of Earth Sciences, University of Minnesota–Twin Cities. This research used resources of the Advanced Photon Source, a U.S. Department of Energy (DOE) Office of Science User Facility operated for the DOE Office of Science by Argonne National Laboratory under Contract No. DE-AC02-06CH11357. A portion of this research used resources at the High Flux Isotope Reactor, a DOE Office of Science User Facility operated by the Oak Ridge National Laboratory. We acknowledge the support of NIST, U.S. Department of Commerce, in providing some of the neutron research facilities used in this work.

[1] M. Mochizuki and M. Imada, New J. Phys. **6**, 154 (2004).
[2] D. A. MacLean, H. N. Ng, and J. E. Greedan, J. Solid State Chem. **30**, 35 (1979).
[3] J. E. Greedan, J. Less-Common Met. **111**, 335 (1985).
[4] H. D. Zhou and J. B. Goodenough, J. Phys.: Condens. Matter **17**, 7395 (2005).
[5] J. P. Goral, J. E. Greedan, and D. A. MacLean, J. Solid State Chem. **43**, 244 (1982).
[6] Y. Okimoto, T. Katsufuji, Y. Okada, T. Arima, and Y. Tokura, Phys. Rev. B **51**, 9581 (1995).
[7] H. D. Zhou and J. B. Goodenough, Phys. Rev. B **71**, 184431 (2005).
[8] S. Hameed *et al.*, Phys. Rev. B **104**, 024410 (2021).
[9] G. Amow, J.-S. Zhou, and J. B. Goodenough, J. Solid State Chem. **154**, 619 (2000).
[10] Y. Tokura, Y. Taguchi, Y. Okada, Y. Fujishima, T. Arima, K. Kumagai, and Y. Iye, Phys. Rev. Lett. **70**, 2126 (1993).
[11] Y. Tokura, Y. Taguchi, Y. Moritomo, K. Kumagai, T. Suzuki, and Y. Iye, Phys. Rev. B **48**, 14063 (1993).
[12] S. Hameed, J. Joe, D. M. Gautreau, J. W. Freeland, T. Birol, and M. Greven, Phys. Rev. B **104**, 045112 (2021).
[13] P. Xu, T. C. Droubay, J. S. Jeong, K. A. Mkhoyan, P. V. Sushko, S. A. Chambers, and B. Jalan, Adv. Mater. Interfaces **3**, 1500432 (2016).
[14] P. Xu, Y. Ayino, C. Cheng, V. S. Pribiag, R. B. Comes, P. V. Sushko, S. A. Chambers, and B. Jalan, Phys. Rev. Lett. **117**, 106803 (2016).
[15] Y. Cao, Z. Yang, M. Kareev, X. Liu, D. Meyers, S. Middey, D. Choudhury, P. Shafer, J. Guo, J. W. Freeland, E. Arenholz, L. Gu, and J. Chakhalian, Phys. Rev. Lett. **116**, 076802 (2016).
[16] S. Raghavan, J. Y. Zhang, and S. Stemmer, Appl. Phys. Lett. **106**, 132104 (2015).
[17] P. Moetakef, J. R. Williams, D. G. Ouellette, A. P. Kajdos, D. Goldhaber-Gordon, S. J. Allen, and S. Stemmer, Phys. Rev. X **2**, 021014 (2012).
[18] M. N. Grisolia, J. Varignon, G. Sanchez-Santolino, A. Arora, S. Valencia, M. Varela, R. Abrudan, E. Weschke, E. Schierle, J. E. Rault, J. P. Rueff, A. Barthélémy, J. Santamaria, and M. Bibes, Nat. Phys. **12**, 484 (2016).
[19] R. Aeschlimann, D. Preziosi, P. Scheiderer, M. Sing, S. Valencia, J. Santamaria, C. Luo, H. Ryll, F. Radu, R. Claessen, C. Piamonteze, and M. Bibes, Adv. Mater. **30**, 1707489 (2018).
[20] R. Aeschlimann, M. N. Grisolia, G. Sanchez-Santolino, J. Varignon, F. Choueikani, R. Mattana, V. Garcia, S. Fusil, T. Fröhlich, M. Braden, B. Delley, M. Varela, P. Ohresser, J. Santamaria, A. Barthélémy, C. Piamonteze, and M. Bibes, Phys. Rev. Materials **5**, 014407 (2021).
[21] A. Najev, S. Hameed, D. M. Gautreau, Z. Wang, J. Joe, M. Požek, T. Birol, R. M. Fernandes, M. Greven, and D. Pelc, arXiv:2105.06695.
[22] S. Hameed *et al.* (unpublished).
[23] Certain commercial equipment, instruments, or materials are identified in this paper in order to specify the experimental procedure adequately. Such identification is not intended to imply recommendation or endorsement by the NIST, nor is it intended to imply that the materials or equipment identified are necessarily the best available for the purpose.
[24] See Supplemental Material at http://link.aps.org/supplemental/10.1103/PhysRevMaterials.5.125003 for XAS measurements in TEY mode and characterization data on additional La substitution and Ca doping levels.
[25] Y. Taguchi, Y. Tokura, T. Arima, and F. Inaba, Phys. Rev. B **48**, 511 (1993).
[26] J. Yue, N. F. Quackenbush, I. Laraib, H. Carfagno, S. Hameed, A. Prakash, L. R. Thoutam, J. M. Ablett, T.-L. Lee, M. Greven, M. F. Doty, A. Janotti, and B. Jalan, Phys. Rev. Materials **4**, 112001(R) (2020).
[27] C. Ulrich, G. Ghiringhelli, A. Piazzalunga, L. Braicovich, N. B. Brookes, H. Roth, T. Lorenz, and B. Keimer, Phys. Rev. B **77**, 113102 (2008).
[28] G. I. Meijer, W. Henggeler, J. Brown, O. S. Becker, J. G. Bednorz, C. Rossel, and P. Wachter, Phys. Rev. B **59**, 11832 (1999).
[29] H. Roth, Single crystal growth and electron spectroscopy of d^1 systems, Doctoral dissertation, Universität zu Köln (2008).
[30] D. K. de Vries and A. D. Wieck, Am. J. Phys. **63**, 1074 (1995).
[31] S. Hameed, D. Pelc, Z. W. Anderson, A. Klein, R. J. Spieker, L. Yue, B. Das, J. Ramberger, M. Lukas, Y. Liu, M. J. Krogstad, R. Osborn, Y. Li, C. Leighton, R. M. Fernandes, and M. Greven, Nat. Mater. **21**, 54 (2022).
[32] D. Wang, C. Huang, J. He, X. Che, H. Zhang, and F. Huang, ACS Omega **2**, 1036 (2017).
[33] C. Zhang, F. Hao, G. Gao, X. Liu, C. Ma, Y. Lin, Y. Yin, and X. Li, npj Quantum Mater. **2**, 2 (2017).
[34] B. Keimer, D. Casa, A. Ivanov, J. W. Lynn, M. V. Zimmermann, J. P. Hill, D. Gibbs, Y. Taguchi, and Y. Tokura, Phys. Rev. Lett. **85**, 3946 (2000).
[35] C. Ulrich, G. Khaliullin, S. Okamoto, M. Reehuis, A. Ivanov, H. He, Y. Taguchi, Y. Tokura, and B. Keimer, Phys. Rev. Lett. **89**, 167202 (2002).